Unsteady Transonic Aerodynamics and Aeroelastic Calculations at Low-Supersonic Freestreams

Guru P. Guruswamy*
Sterling Federal Systems, Inc., Palo Alto, California
and
Peter M. Goorjian†
NASA Ames Research Center, Moffett Field, California

A computational procedure is presented to simulate transonic unsteady flows and corresponding aeroelasticity of wings at low-supersonic freestreams. The flow is modeled by using the transonic small-perturbation theory. The structural equations of motions are modeled using modal equations of motion directly coupled with aerodynamics. Supersonic freestreams are simulated by properly accounting for the boundary conditions based on pressure waves along the flow characteristics in streamwise planes. The flow equations are solved using the time-accurate, alternating-direction implicit finite-difference scheme. The coupled aeroelastic equations of motion are solved by an integration procedure based on the time-accurate, linear-acceleration method. The flow modeling is verified by comparing calculations with experiments for both steady and unsteady flows at supersonic freestreams. The unsteady computations are made for oscillating wings. Comparisons of computed results with experiments show good agreement. Aeroelastic responses are computed for a rectangular wing at Mach numbers ranging from subtransonic to upper-transonic (supersonic) freestreams. The extension of the transonic dip into the upper transonic regime is illustrated.

Introduction

FLYING aircraft in the transonic regime is efficient because of the high lift-to-drag ratios. However, several undesirable phenomena occur in the transonic regime. From an aeroelastic point of view, the major concern is the presence of moving shock waves and the rapid changes in the flows because of structural deflections. One commonly observed undesirable phenomenon in the transonic regime is the dip in the flutter curve.[1,2]

The nonlinear flow effects in the transonic regime have proven to be challenging for both experiments and computations. To date, the most advanced codes for practical aeroelastic applications use equations based on the potential flow theory. Methods based on Euler/Navier-Stokes equations are just becoming useful for practical applications.

Among potential flow theories, procedures based on the transonic small-perturbation (TSP) theory have lead to the development of successful computational methods for three-dimensional flows.[3,4] A finite-difference scheme based on the alternate-direction implicit scheme combined with the Murman-Cole shock-capturing method has proven successful in providing time-accurate, unsteady transonic results for wings and wing/body configurations.[5] Using this time-accurate finite-difference technique, TSP equations have been solved to date for transonic flows with only subsonic freestreams.[3,4]

However, flows can be transonic for supersonic freestream Mach numbers near unity. Experimental studies[1] for wings have shown that the transonic dip phenomenon can extend into the upper transonic regime with supersonic freestreams. Therefore, there is a need for an efficient computational method that can compute nonlinear flowfields in the upper transonic regime. A time-accurate procedure based on the alternate-direction implicit (ADI) scheme for unsteady transonic airfoil calculations at supersonic freestreams was first presented in Ref. 6. In the present work, a similar procedure for three-dimensional flows is presented for wings. The present procedure is also coupled with structural equations of motion by using a simultaneous integration procedure[7] and it is incorporated in XTRAN3S-Ames[4] code, the Ames version of the Air Force/NASA XTRAN3S.[8] Recently, unsteady transonic computations at supersonic freestreams were made for wings using a finite-difference scheme based on the approximate factorization (AF) method in Ref. 9.

The present work is done in conjunction with further extension of XTRAN3S, a general-purpose code that is being developed for computing unsteady transonic aerodynamics and aeroelasticity of full aircraft. At present, this code can be used to compute flows over wings and full-span wing/body configurations with tip-mounted missiles and with active control surfaces. Because of the use of the TSP equation, the computational time is practical for computationally intensive aeroelastic calculations. The present development will extend the capability of XTRAN3S to a full transonic range.

In this paper, a scheme that can be used to compute the full range of transonic flows is presented. The basic solution procedure is based on an alternating-direction, finite-difference scheme, combined with the Murman-Cole shock-capturing technique. The far-field boundary conditions are varied depending on the freestream Mach numbers. For subsonic freestreams, boundary conditions are used from subsonic theory.[3] For supersonic freestreams, boundary conditions are switched to those from supersonic theory. Steady and unsteady flows are computed for rectangular and fighter wings at supersonic freestreams. Computed results are compared with the corresponding experimental data. Aeroelastic response analysis is conducted for a rectangular wing. The extension of the transonic dip into the supersonic regime is illustrated.

Formulation of Unsteady Transonic Flow Equations

The three-dimensional modified, small-disturbance, unsteady transonic equation of motion used in this analysis is given by

$$A\phi_{tt} + B\phi_{xt} = [E\phi_x + F\phi_x^2 + G\phi_y^2]_x + [\phi_y + H\phi_x\phi_y]_y + [\phi_z]_z \quad (1)$$

Received Dec. 14, 1987; revision received May 18, 1988.

*Principal Analyst. Associate Fellow AIAA.
†Research Scientist. Associate Fellow AIAA.

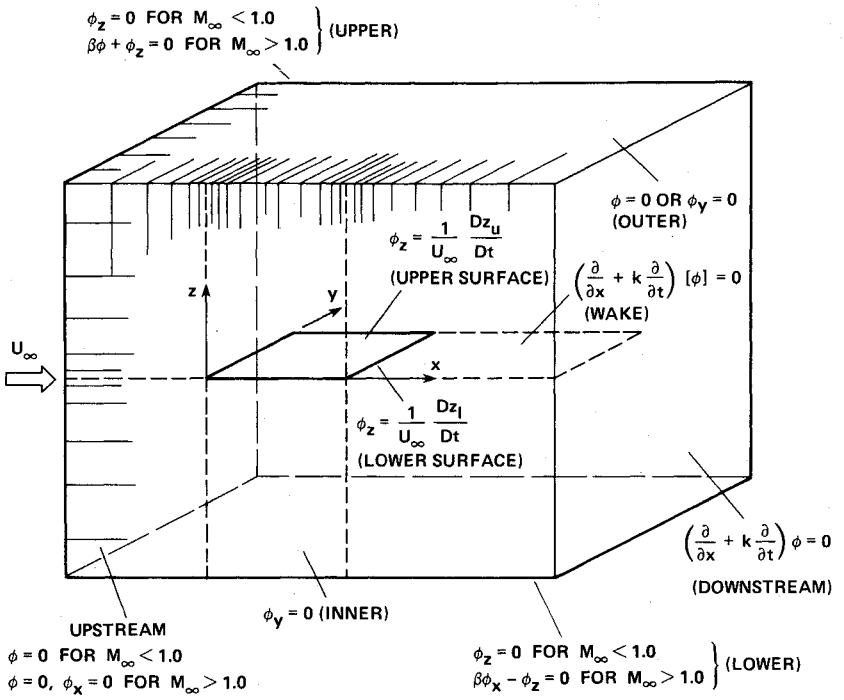

Fig. 1 Flow and wing boundary conditions.

where

$$A = M_\infty^2;\ B = 2M_\infty^2$$

$$E = (1 - M_\infty^2);\ F = -(\tfrac{1}{2})(\gamma + 1)M_\infty^2$$

$$G = -(\tfrac{1}{2})(\gamma - 3)M_\infty^2;\ H = -(\gamma - 1)M_\infty^2$$

The thin-wing, surface flow tangency condition satisfied at the mean plane is given by

$$\phi_z = f_x + kf_t \tag{2}$$

where $f(x)$ denotes the airfoil surface and k a time scale.

Jump conditions used for the trailing vortex wake are

$$[\phi_z] = 0 \tag{3a}$$

$$[\phi_x + k\phi_t] = 0 \tag{3b}$$

where [ ] denotes the jump in the quantity across the vortex sheet.

Far-Field Boundary Conditions

For subsonic freestreams, the boundary conditions from the TSP theory are implemented. For supersonic freestreams, the numerical far-field boundary conditions are modified to reflect the physical domain of dependence and to enhance the stability characteristics of the numerical scheme. In this work, modifications are implemented only in the flow boundaries of streamwise planes following the development in Ref. 6. The wall and far-span boundaries are not modified. This type of boundary conditions are adequate since the purpose of the present study is to make computations at low supersonic Mach numbers when the flow is still transonic on the wing. Numerical experiments in this study have shown the validity of these boundary conditions.

Upstream Boundary Conditions

At the upstream boundary, the flow is uniform and unperturbed. Thus, the disturbance velocity potential is zero and the upstream boundary conditions for the subsonic freestream are

$$\phi = 0 \tag{4a}$$

and for the supersonic freestream

$$\phi = 0 \tag{4b}$$

$$\phi_x = 0 \tag{4c}$$

Downstream Boundary Conditions

Such conditions for the subsonic freestream are

$$\phi_x + k\phi_t = 0 \tag{5a}$$

and for the supersonic freestream

$$\beta\phi_x + \phi_z = 0 \quad \text{for } z > 0.0 \tag{5b}$$

$$\beta\phi_x - \phi_z = 0 \quad \text{for } z < 0.0 \tag{5c}$$

At far-fields above and below the wing, the condition for the subsonic freestream is

$$\phi_z = 0 \tag{6a}$$

and for the supersonic freestream

$$\beta\phi_x + \phi_z = 0 \text{ at boundary above the wing} \tag{6b}$$

$$\beta\phi_x - \phi_z = 0 \text{ at boundary below the wing} \tag{6c}$$

where $\beta = (M_\infty^2 - 1)^{1/2}$. These conditions are obtained from the supersonic linear theory and correspond to the propagation of pressure waves along the flow characteristics, which are lines of constant velocity potential.

At wing root and far-span, for both subsonic and supersonic freestreams, the condition is

$$\phi_y = 0 \tag{7}$$

The above flowfield boundary conditions and wing surface boundary conditions are illustrated in Fig. 1.

Transformation of Aerodynamic Equations

The aerodynamic equations are transformed so that a swept-tapered wing can be analyzed by using a finite-differ-

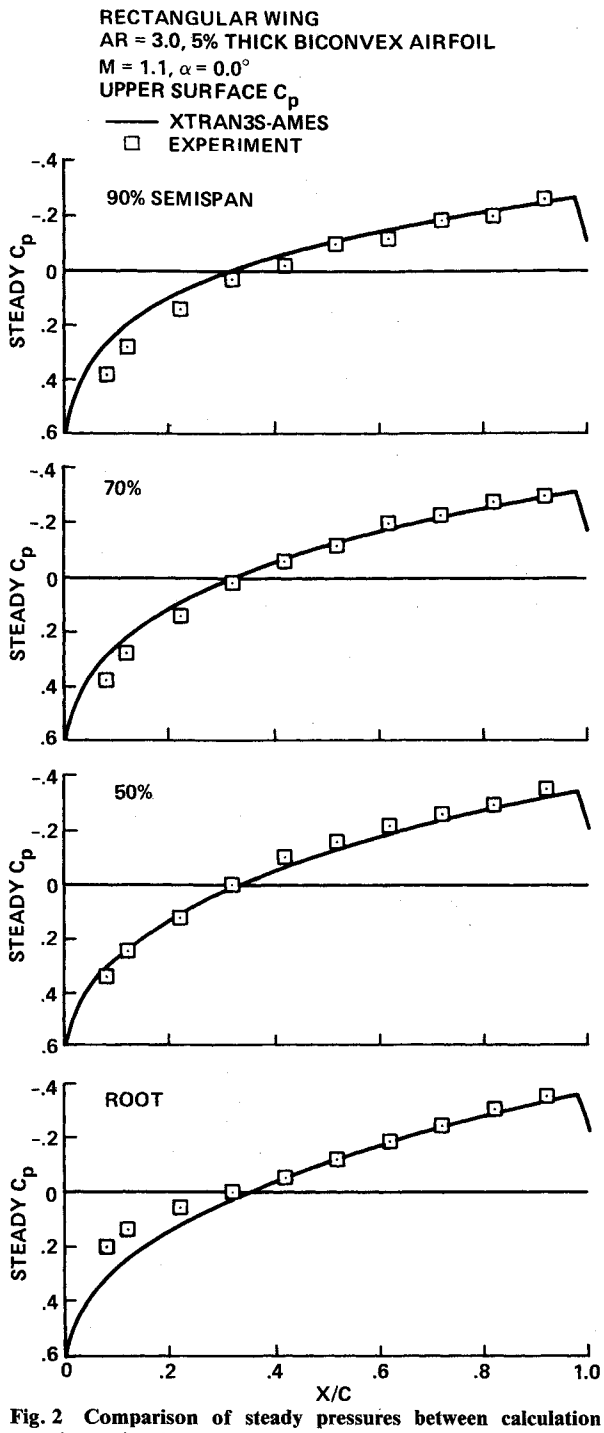

Fig. 2 Comparison of steady pressures between calculation and experiment for the rectangular wing.

ence mesh that is aligned with the leading and trailing edges of the wing. The transformed equation is obtained by the modified shearing transformation[4] solved by the time-accurate, alternating-direction, implicit finite-difference scheme. The transformation that maps a swept-tapered wing to a rectangular planform is given by

$$\xi = \xi(x,y) \tag{8a}$$

$$\eta = y \tag{8b}$$

$$\zeta = z \tag{8c}$$

where Eq. (8a) is obtained by using the Ames-modified shearing transformation.[4] The resulting transformed equation is given by

$$-[A\xi_x^{-1}\phi_t + B\phi_\xi]_t = [E\xi_x\phi_\xi + F\xi_x^2\phi_\xi^2 + G(\xi_y\phi_\xi + \phi_\eta)^2 + \xi_x^{-1}\xi_y(\xi_y\phi_\xi + \xi_y + \phi_\eta) + H\xi_y\phi_\xi(\xi_y\phi_\xi + \phi_\eta)]_\xi + [\xi_x^{-1}(\xi_y\phi_\xi + \phi_\eta) + H\phi_\xi(\xi_y\phi_\xi + \phi_\eta)]_\eta + [\xi_x^{-1}\phi_\xi]_\xi = 0 \tag{9}$$

The differencing procedure for Eq. (9) is an extension of the Murman-Cole type-dependent difference procedure applied to an arbitrary coordinate system.[3]

Aeroelastic Equations of Motion

The governing aeroelastic equations of motion of a flexible wing are obtained by using the Rayleigh-Ritz method. In this method, the resulting aeroelastic displacement at any time are expressed as a function of a finite set of selected modes. The contribution of each selected mode to the total motion is derived by Lagrange's equation. Furthermore, it is assumed that the deformation of the continuous wing structure can be represented by deflections at a set of discrete points. This assumption facilitates the use of discrete structural data, such as the modal vector, modal stiffness matrix, and modal mass matrix. In this study, the finite-element method is employed to obtain the modal data.

It is assumed that the deformed shape of the wing can be represented by a set of discrete displacements at selected nodes. From the modal analysis, the displacement vector $\{d\}$ can be expressed as

$$\{d\} = [\phi]\{q\} \tag{10}$$

where $[\phi]$ is the matrix of displacements of the natural vibration modes interpolated to the finite-difference grid points used to model the flow and $\{q\}$ the generalized displacement vector.

The final matrix form of the aeroelastic equations of motion is

$$[M]\{\ddot{q}\} + [G]\{\dot{q}\} + [K]\{q\} = \{F\} \tag{11}$$

where $[M]$, $[G]$, and $[K]$ are the modal mass, damping, and stiffness matrices, respectively, and $\{\dot{q}\}$ and $\{\ddot{q}\}$ the generalized velocity and acceleration vectors, respectively. $\{F\}$ is the aerodynamic force vector defined as $(\frac{1}{2})\rho U_\infty^2[\phi]^T[A]\{\Delta C_p\}$ and $[A]$ the diagonal area matrix of the aerodynamic control points, which are same as the grid points used for the finite-difference modeling of the flow.

The matrix $[A]$ is computed as follows. Each finite-difference grid cell is divided into four equal subcells. The component of the area matrix $[A]$ associated with any grid point is computed by adding the areas of all the subcells adjoining to that grid point. Interior grid points have four subcells per grid point. The wing boundary grid points have two subcells per grid point.

The aeroelastic equations of motion [Eq. (11)] are solved by numerically integrating in time by the linear acceleration method.[7] The step-by-step integration procedure for obtaining the aeroelastic response was performed as follows. Assuming that freestream conditions and wing surface boundary conditions were obtained from a set of selected starting values of the generalized displacement, velocity, and acceleration vectors, the generalized aerodynamic force vector $F(t)$ at time $t + \Delta t$ was computed by solving Eq. (11). Using this aerodynamic vector, the generalized displacement, velocity, and acceleration vectors for the time level $t + \Delta t$ are calculated by numerically integrating Eq. (9). From the generalized displacements computed at the time level $t + \Delta t$, the new boundary conditions on the surface of the wing are computed. With these new boundary conditions, the aerodynamic vector $F(t)$ at the next

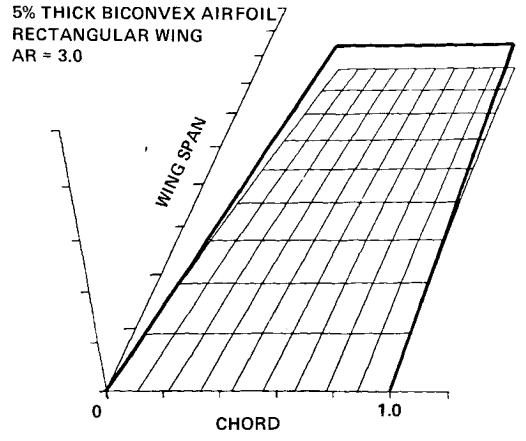

Fig. 3 First bending mode of the rectangular wing for unsteady computations.

time level is computed by using Eq. (9). This process is repeated at every time step to solve the aerodynamic and structural equations of motion forward in time until the required response is obtained.

Results

Aerodynamic Computations

Transonic steady and unsteady pressures were computed for a rectangular wing and a fighter wing at supersonic freestreams. For all the cases considered in this work, a grid with 64 points in the x direction, 20 points in the y direction, and 40 points in the z direction was used in the analysis. The unsteady pressures were computed by forcing the wing to undergo a sinusoidal modal motion for three cycles of 360 time steps per cycle during which time the transients disappeared and a periodic response was obtained. All computed results are compared with the corresponding experimental data.

The rectangular wing selected has an aspect ratio of 3, with 5% thick biconvex airfoil sections. Both steady and unsteady experimental data are available for this wing from wind-tunnel tests.[10] Both steady and unsteady transonic pressure results computed by using Eq. (9) compare well with the experiments at subsonic freestreams. Here, results at supersonic freestreams are presented.

In Fig. 2, the steady pressures are compared between the theory and the experiment at $M = 1.1$ for four span stations. The two sets of data compare well at all span stations. The computed result shows the presence of a shock wave near the trailing edge. For this wing, the unsteady pressures were measured in the wind tunnel when the wing was oscillating in its first bending mode as shown in Fig. 3. The same modal motion was simulated in the calculation. In Fig. 4, magnitudes and phase angles of the unsteady pressure jumps obtained by the computation and the experiment are plotted at 0, 50, 70, and 90% semispan stations, respectively, for $M = 1.1$ and $k = 0.22$. The magnitudes of the pressure coefficients compare better than the phase angles. The discrepancies near the root are possibly due to the viscous effects of the wall that were not considered in the computed results. The discrepancies for span stations away from the wall are due to the scattered experimental data. However, the computed and experimental results agree fairly well in trend.

The selected fighter wing was the F-5 wing with an aspect ratio of 3, for which both steady and unsteady data are available from wind tunnel tests.[11] Both steady and unsteady transonic pressure results computed by using Eq. (9) compare well with the experiments at subsonic freestreams.[4]

In Fig. 5, the steady pressure curves are compared between the theory and the experiment for $M = 1.33$ at four spanwise stations. The two sets of data compare well at all span stations. The computed result shows the presence of a shock wave near the trailing edge. Figure 6 shows the modal motion

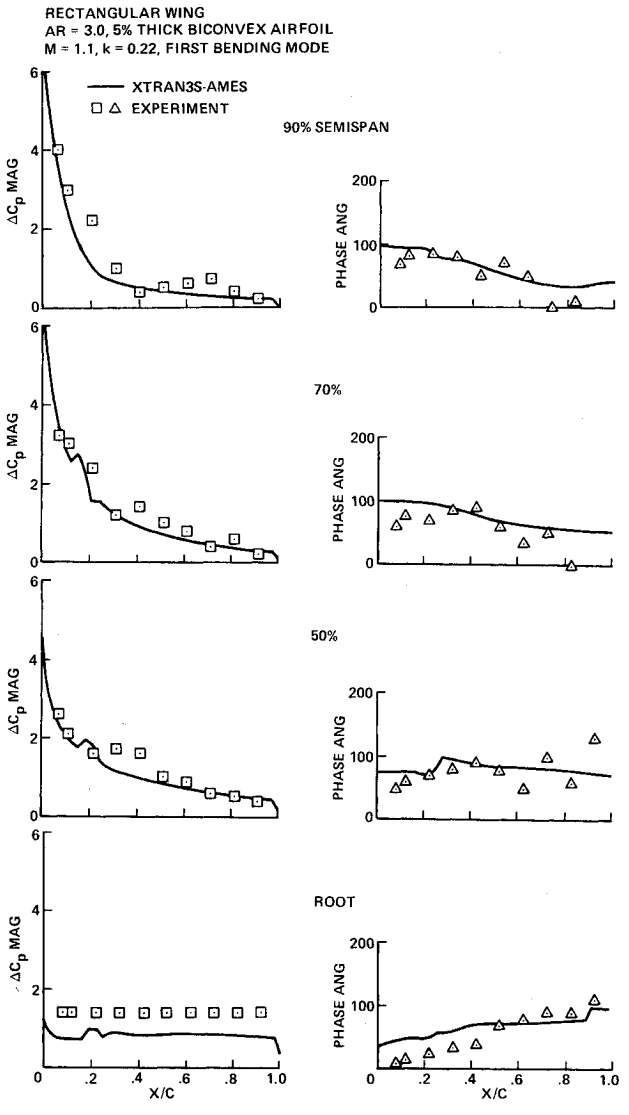

Fig. 4 Comparison of unsteady pressures between calculation and experiment for the rectangular wing.

used in the experiment.[12] The wing is pitching about an axis located at the 50% root chord and the pitching axis is normal to the wing root. Figure 7 shows plots of the real and imaginary values of the upper-surface pressures at four span stations obtained by the present study and the experiment at a supersonic freestream of $M = 1.34$. These results were obtained for the wing oscillating at a frequency of 40 cycles. The same modal motion used as in the experiment was simulated in the calculation. As shown in Fig. 7, both the real and imaginary parts of the computed unsteady pressures compare well with the experiment for all span stations. Some discrepancies between the results may be due to the viscous effects that are not accounted for in the computations.

Aeroelastic Computations

To illustrate an aeroelastic case, a typical uniform rectangular wing of aspect ratio 5.0 with 6% thick parabolic arc sections was selected. Transonic flutter characteristics of this wing are available from the wind-tunnel tests.[12] The mode shapes and frequencies required for the modal equations of motion [Eq. (11)] were obtained by a 16-degree-of-freedom rectangular finite element.[13] Figure 8 shows the mode shapes and frequencies of the first five natural modes for the wing. The modal data compare well with the measured data from the wind-tunnel flutter tests.[12] For example, the computed values of the natural frequencies of the first bending and torsional modes are 13.21 and 67.32 H_z, respectively. The correspond-

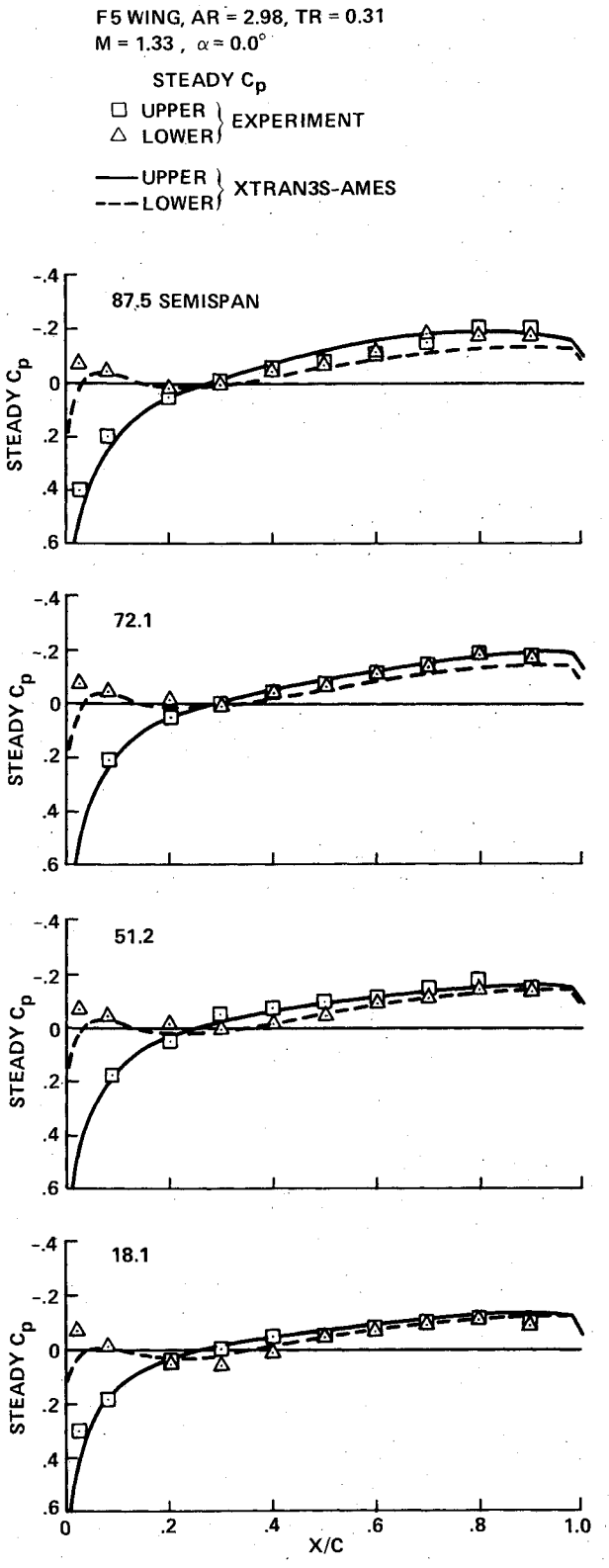

Fig. 5 Comparison of steady pressures between calculation and experiment of the F-5 wing.

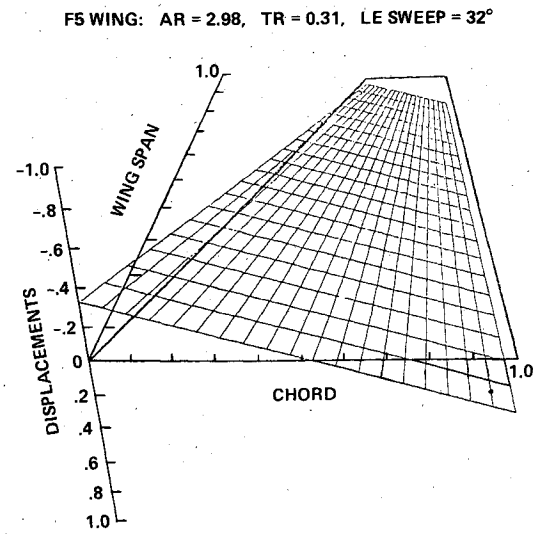

Fig. 6 Modal motion of the F-5 wing for unsteady computations.

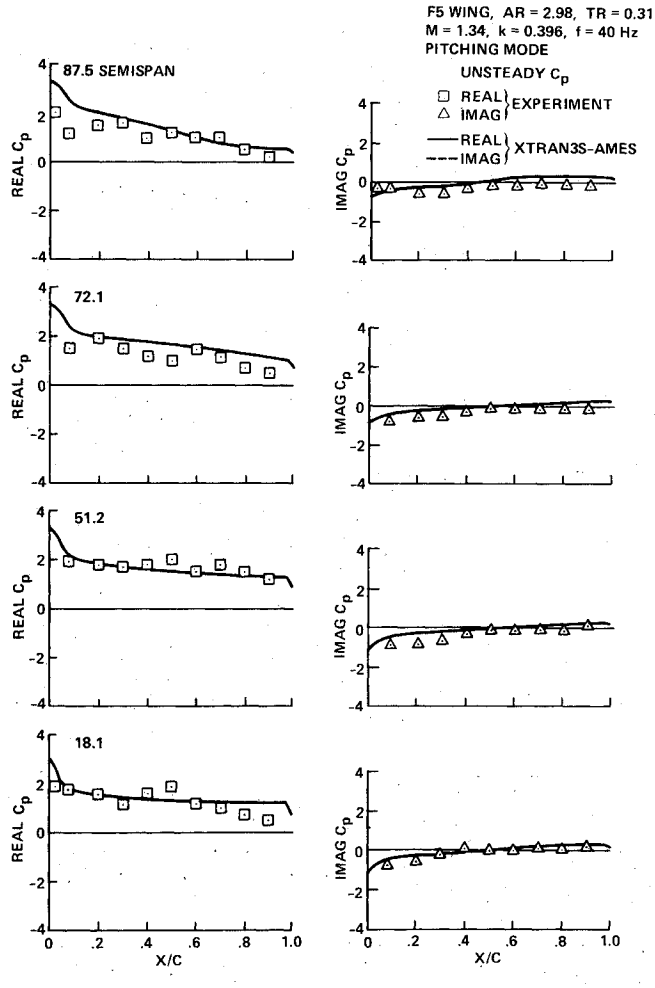

Fig. 7 Comparison of upper-surface unsteady pressures between calculation and experiment for the F-5 wing.

ing measured values are 14.29 and 80.40 H_z, respectively. The computed values were obtained using the structural properties of the aluminum-alloy flat-plate insert in the model. The influence of the lightweight covering used for the wind-tunnel model to provide the thickness was not accounted for in the computations due to lack of available data. This might have caused discrepancies between the computed and measured frequencies. Using these modal data, the aeroelastic equation of motion [Eq. (11)] was solved.

Aeroelastic analyses were conducted for Mach numbers from lower transonic of about 0.70 to upper transonic of about 1.1. All responses were started with modally displaced initial conditions obtained by giving unit values to the first two generalized displacements, $q(1)$ and $q(2)$. Mach numbers selected represent flow conditions ranging from subsonic, to transonic with shock waves, to transonic at supersonic free-streams. In Figs. 9–11, the responses of the first and second generalized displacements $q(1)$ and $q(2)$ of Eq. (11) are shown

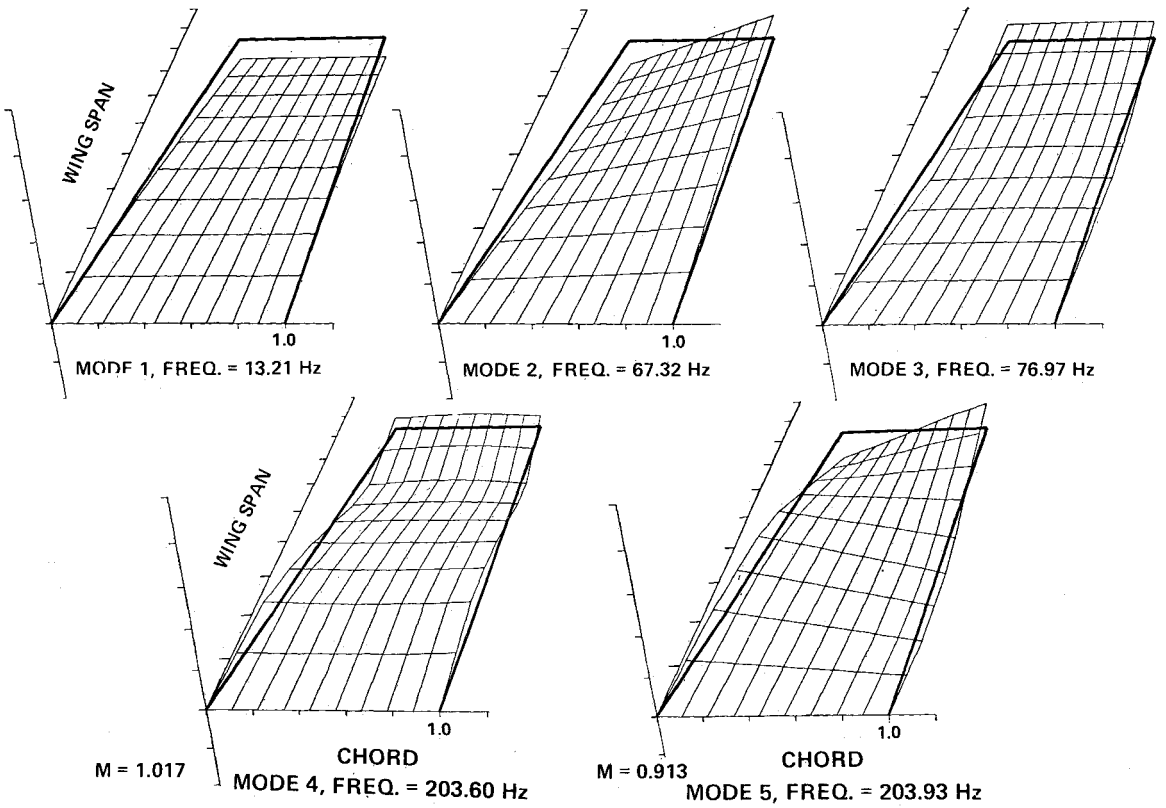

Fig. 8 Mode shapes of the rectangular wing for aeroelastic analysis.

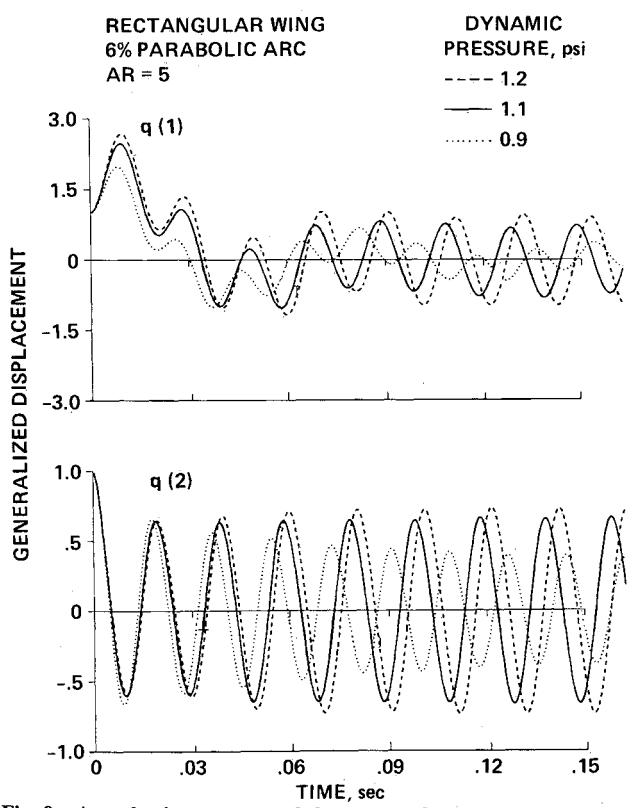

Fig. 9 Aeroelastic responses of the rectangular wing at $M = 0.913$.

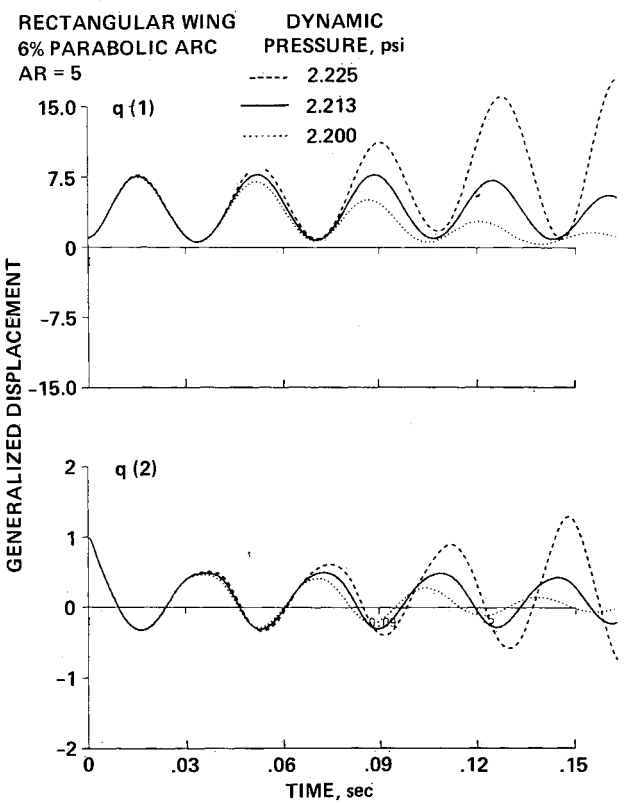

Fig. 10 Aeroelastic responses of the rectangular wing at $M = 1.017$.

for Mach numbers 0.913, 1.017, and 1.1, respectively. For each Mach number, responses that are stable, near neutrally stable, and unstable are shown by varying the dynamic pressures. From these results, the responses are more sensitive to the variation of dynamic pressure at supersonic freestreams than at subsonic freestreams. For example, increases in dynamic pressures of about 25 and 10% were required for the response to go from stable to unstable conditions for $M = 0.913$ and 1.100, respectively.

The flutter speeds were computed by numerically interpolating the dynamic pressures to match a response that corresponds to zero damping. This was accomplished by fitting a

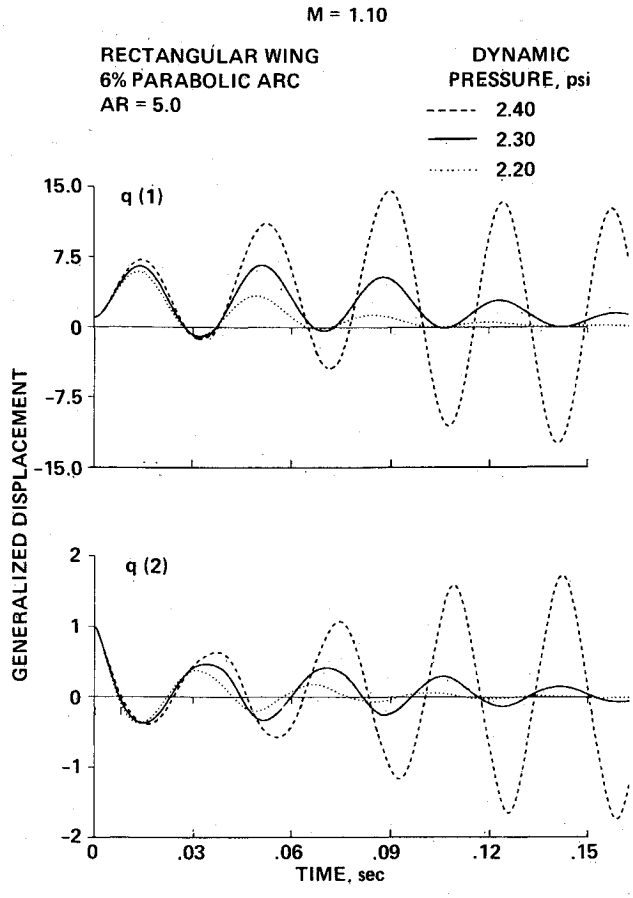

Fig. 11 Aeroelastic responses of the rectangular wing at $M = 1.100$.

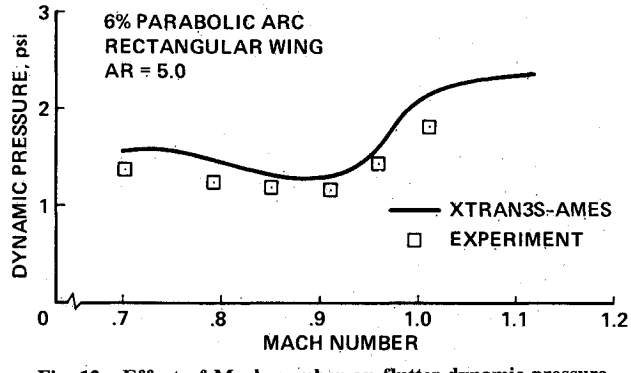

Fig. 12 Effect of Mach number on flutter dynamic pressure.

quadratic curve between the dynamic pressures and damping coefficients using the responses of the first generalized coordinate $q(1)$ computed at three dynamic pressures. Since the configuration considered is a simple rectangular wing, only the responses of $q(1)$ were adequate in determining the flutter dynamic pressure. In order to compute the flutter dynamic pressure accurately, dynamic pressures were chosen close to the possible flutter dynamic pressure. In this work, such a selection was possible since the flutter dynamic pressures were approximately known from the wind-tunnel measurements. In other situations where such experimental data are not available, approximate flutter dynamic pressures can be found using the uncoupled flutter analysis that is computationally less expensive than the present time response analysis. Such a procedure is explained by Guruswamy and Yang.[7]

The plots of dynamic pressure vs Mach number from both computations and the experiment[12] are shown in Fig. 12. The computed flutter speeds, which compare well with the experiment, show a slightly less conservative flutter boundary. The transonic dip in the flutter curve that extends to the zone of supersonic freestreams can be seen in the figure. These aeroelastic results illustrate the importance of the method presented in this paper for computing transonic flows at supersonic freestreams.

Conclusions

A procedure has been developed for computing unsteady transonic aerodynamic loads at supersonic freestreams. The flow is modeled using the transonic small-disturbance equations of motion. Steady and unsteady pressure distributions for both rectangular and fighter wings compare well with experiments. Aeroelastic computations were made for a rectangular wing by simultaneously integrating unsteady aerodynamics and structural equations of motion. The computed flutter results compare well with the wind-tunnel measured data. The extension of the transonic dip into the supersonic freestream zone and also the sensitivity of the responses at supersonic freestreams are illustrated. The present time-accurate simulation is close to wind-tunnel simulation and can be an efficient compliment to wind-tunnel/flight tests for reducing design cost.

Acknowledgments

This work was supported through funding from the Flight Dynamics Laboratory, Air Force Wright Aeronautical Laboratories, Wright Patterson AFB and was monitored by Messrs. Larry Huttsell and Dale Cooley of the Aeroelastic Group. The authors appreciate many helpful suggestions made by Mr. Huttsell during the course of this work.

References

[1]Farmer, M. G. and Hanson, P. W., "Comparison of Supercritical and Conventional Wing Flutter Characteristics," NASA TM X-72837, May 1976.

[2]Ashley, H., "Role of Shocks in the 'Sub-Transonic' Flutter Phenomenon," *Journal of Aircraft*, Vol. 17, March 1980, pp. 187-197.

[3]Borland, C. J. and Rizzetta, D. P., "Nonlinear Transonic Flutter Analysis About Airfoils," *AIAA Journal*, Vol. 20, Nov. 1982, pp. 1606-1615.

[4]Guruswamy, P. and Goorjian, P. M., "Efficient Algorithm for Unsteady Transonic Aerodynamics of Low-Aspect Ratio Wings," *Journal of Aircraft*, Vol. 22, March 1985, pp. 193-199 (also AIAA Paper 84-0872, May 1984).

[5]Guruswamy, G. P. and Goorjian, P. M., "Unsteady Transonic Flow Simulation on a Full-Span Wing-Body Configuration," AIAA Paper 87-1240, June 1987.

[6]Chow, L. J. and Goorjian, P. M., "Implicit Unsteady Transonic Airfoil Calculations at Supersonic Freestreams," AIAA Paper 82-0934, June 1982.

[7]Guruswamy, P. and Yang, T. Y., "Aeroelastic Time Response Analysis of Thin Airfoils by Transonic Code LTRAN2," *Computers and Fluids*, Vol. 9, Dec. 1980, pp. 409-425.

[8]Huttsell, L. J. and Cooley, D. E., "The Background and Status of the Joint Air Force/NASA Transonic Unsteady Aerodynamic Program (XTRAN3S)," AFWAL TM-86-154-FIBRC, Jan. 1986.

[9]Bennett, R. M., Bland, S. R., Batina, J. T., Gibbons, M. D. and Mabey, D. G., "Calculation of Steady and Unsteady Pressures on Wings at Supersonic Speeds with a Transonic Small Disturbance Code," AIAA Paper 87-0851, April 1987.

[10]Lessing, H. C., Troutman, J. L., and Menees, G. P., "Experimental Determination of the Pressure Distribution on a Rectangular Wing Oscillating in First Bending Mode for Mach Numbers from 0.24 to 1.30," NASA TN D-344, Dec. 1960.

[11]Tijdeman, J. et al., "Transonic Wind Tunnel Tests on an Oscillating Wing with External Stores; Part II-The Clean Wing," AFFDL-TR-78-194, March 1979.

[12]Dogget, R. V., Rainey, A. G., and Morgan, H. G., "An Experimental Investigation of Aerodynamic Effects of Airfoil Thickness on Transonic Flutter Characteristics," NASA TM X-79, 1959.

[13]Guruswamy, P. and Yang, T. Y., "Special-Purpose Finite Element Programs," *Finite Element Structural Analysis*, by T. Y., Yang, Prentice Hall, Englewood Cliffs, NJ, 1986, Chap. 13.